ACS OMEGA

http://pubs.acs.org/journal/acsodf

Article

Humic Acid Extracted from Danty via Catalytic Oxidation Using H_2O_2/Birnessite: Characteristics and Agricultural Beneficial Effects

Zixin Zhang, Qi Chen,* Guohua Ma, Kexin Zhang, Zhaoming Qu, Gaoyang E, Conghui Wang, Peng Zhang, Zhiguang Liu, Min Zhang, and Jibiao Geng*

Cite This: *ACS Omega* 2022, 7, 47192−47201

Read Online

ACCESS | Metrics & More | Article Recommendations | Supporting Information

ABSTRACT: Extraction optimization is very important for the quality of humic acid (HA). In this study, actived HA (HA_b) was extracted from danty via catalytic oxidation using birnessite as a catalyst and H_2O_2 as an oxidant. Single-factor experiments and the response surface method were used to optimize the acidic functional group content of HA_b. It was found that the maximum acidic functional group content of HA_b can be achieved when danty-crushing time, H_2O_2 concentration, and birnessite dose were 105.7 min, 20, and 2%, respectively. Fourier transform infrared spectra showed that HA_b had more surface functional groups than commercial HA (HA_c) and HA extracted using the traditional method of the International Humic Substances Society (HA_I). In addition, acidic functional group titration showed that HA_b had 84.3% more acidic functional groups and 118.9% more carboxyl groups than HA_I. Additionally, HA_b had the greatest effect on promoting the dissolution of carbonate and bicarbonate, promoting the settlement of calcaline alkaline soil, and improving the germination rate of wheat seeds under saline and alkaline stress. This study provides a basis for the efficient extraction of active HA with rich functional groups and its application in agriculture and many other fields.

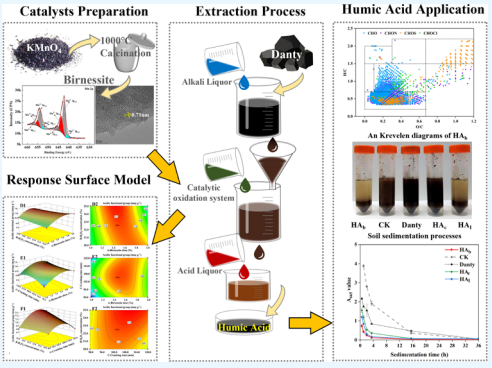

1. INTRODUCTION

Humic acid (HA), a mixture of macromolecular organic acids generated during microbial degradation and transformation of animal and plant remnants,[1,2] is made up of aromatics, aliphatics, and other components.[2] HA possesses a variety of functional groups, including quinones, hydroxyl, carbonyl, phenolic and alcoholic hydroxyls, and methoxyl.[3] Of all the functional groups, the acidic ones of phenolic hydroxyl and carboxyl contribute extremely greatly to the exceptional complexing and ion-exchanging capacities of HA.[4]

In recent years, HA has been broadly applied as a soil conditioner.[5] The addition of HA can increase soil organic matter content and improve soil physical, chemical, and biological properties, thereby promoting plant growth and increasing plant yield.[6,7] The soil quality- and crop yield-promoting effects of HA are especially significant for such soils as calcareous soil and saline−alkali soil, which are of low fertility and productivity.[7,8]

The currently widely employed International Humic Substances Society (IHSS) method of HA extraction is alkaline extraction with NaOH solution, followed by HA precipitation at low pH.[9] However, it is difficult to control the molecular weight[10] and functional group content[11] of HA products due to the weathering degree of raw materials and extraction methods. Therefore, much of the research focuses on optimizing the HA structure and improving HA activity. Tang et al. tried to activate the chemical activity of HA through solid-phase activation;[12] Zhang et al. proposed a new sequential dissolution method to control the composition and structure of HA;[10] Sarlaki et al. purified HA by using membrane ultrafiltration.[13] However, these studies only compared the chemical activities of HA before and after activation and did not carry out quantitative research and application verification.

In this study, an oxidant (i.e., H_2O_2) and a catalyst (i.e., birnessite) were integrated to the IHSS HA extraction method to obtain HA with rich functional groups and of low molecular weight. Birnessite, as a manganese oxide with active properties, was mainly used to remove heavy metals[14,15] in the environment (water environment, atmospheric environment), degradation of organic pollutants,[16,17] and sterilization[18,19]) and others in the field of catalytic degradation. The activation of HA molecules is closely related to the oxidation of side chain groups and the degradation of macromolecular structures. We discovered that birnessite has excellent degradation and catalytic properties, and

Received: October 4, 2022
Accepted: November 29, 2022
Published: December 8, 2022

for the first time, birnessite was used as a catalyst and H_2O_2 as an oxidant in the extraction process of HA.

Transmission electron microscopy (TEM), X-ray diffraction (XRD), X-ray photoelectron spectroscopy (XPS), hydrogen temperature-programmed reduction (H_2-TPR), and oxygen temperature-programmed desorption (O_2-TPD) were employed to study the morphology, structure, and physicochemical properties of the birnessite prepared in this study. Single-factor experiments were first conducted to find out the optimal H_2O_2 concentration, birnessite dose, and danty crushing time for maximum acidic functional group content of the extracted HA. Then, the response surface method was used to fine-tune the above three factors. Finally, the effects of the extracted HA on the sedimentation and carbonate and bicarbonate dissolution of a calcareous soil were investigated. An experiment was also conducted to investigate the effect of the extracted HA on wheat seed germination under salt and alkaline stresses. This study proposes a new method for extracting HA with highly acidic functional group contents. Such HA can improve soil quality, which is especially important for soils with poor structure, low fertility, and low productivity, such as calcareous and saline−alkali soils.

2. MATERIALS AND METHODS

2.1. Materials. The danty used for HA extraction was purchased from Xindeli Power Supply Technology Co. Ltd, Shandong, China. Analytical grade reagents including $KMnO_4$, H_2O_2, HCl, and NaOH were purchased from Tianjin Kaitong Chemical Industry Co., Ltd., Tianjin, China. The commercial HA (HA_c) was purchased from Shandong Xindeli Power Supply Technology Co., Ltd., Shandong, China. All solutions used in this study were prepared with deionized water. The soil samples were obtained from Huantai, Shandong Province, and classified into Aquic Ustochrepts by the US Department of Agriculture's Soil System Classification (ST, 2010). The soil's physical and chemical characteristics are as follows: pH: 8.20 (1:2.5 soil to water ratio) and organic matter content: 16.29 g kg^{-1}, Olsen−P: 9.78 mg kg^{-1}, NO_3^-−N: 11.97 mg kg^{-1}, and NH_4^+−N: 4.49 mg kg^{-1}.

2.2. Birnessite Preparation and Characterization. For birnessite preparation, 4 g $KMnO_4$ was ground and then put in a muffle furnace. The temperature was ramped to 1000 °C in the first 2 h and held for 5 h. After cooled to room temperature, the prepared birnessite was washed with deionized water several times, dried at 105 °C to constant weight, and stored for later use.[20]

TEM images of the prepared birnessite were obtained with a field emission transmission electron microscope (Tecnai G2 F20, USA) at a working voltage of 200 kV. XRD analysis of the prepared birnessite was performed using an X-ray diffractometer (D8-Advance, Bruker, Germany) with Ni-filtered Cu Kα radiation (λ = 1.54 Å), scanning from 5° to 80° 2θ at a scan rate of 1° min^{-1}. O_2-TPD was carried out using an AutoChemll 2920 (USA) apparatus equipped with a TCD detector. H_2-TPR was performed using a ChemiSorb 2720 (USA) apparatus equipped with a TCD detector. The heating rate was 5 °C min^{-1}, and 10 vol % H_2−Ar mixture was used at a flow rate of 15 mL min^{-1}. XPS was obtained on a Thermo escalab 250Xi (USA), using a monochromatic Al Kα radiation source.

2.3. HA Extraction via Catalytic Oxidation and Acidic Functional Group Optimization. Danty was crushed using a Retsch MM400 mixer MILL (Verder Instruments and Equipment Co., Ltd., Germany) at 30 r s^{-1}. Then, 5 g of the crushed danty was mixed with the prepared birnessite, and 25 mL H_2O_2 was added to the mixture. After 30-min reaction at room temperature, 0.5 mol L^{-1} NaOH was added at a solid−liquid ratio of 1:10, and the reaction was carried out at 60 °C for 45 min.[21] Then, centrifuged at 3200 r min^{-1} for 15 min to separate the alkali-soluble HA from the insoluble substances. The supernatant was adjusted to pH 1 with 6 mol L^{-1} HCl to precipitate the HA,[22,23] and the obtained HA was vacuum-dried at 65 °C to constant weight.[13] To dissolve and remove the impurities, the HA powder was washed several times with deionized water (Figure S1). Ensure that there was no residual HCl in the sample until the pH of the HA aqueous solution was greater than 6 (Figure S2A,B).

To maximize the acidic functional group content of HA, single-factor experiments were first performed at the same vibrational frequency and different danty crushing times (0, 30, 60, 90, 120, and 150 min), H_2O_2 concentrations (0.5, 1, 5, 10, 20, and 25%), and birnessite doses (0.3, 0.5, 0.7, 0.9, 1.5, and 2.0%). The three groups of single-factor test parameters are shown in Table S1. Then, a three-factor three-level response surface design (Table S2) was adopted based on the BOX−Behnken design of response surface methodology (RSM) to fine-tune the three factors using the Design-Expert software (V8.0.6, State-Ease Inc., Minneapolis, USA).[24] The HA obtained under the optimal danty crushing time, H_2O_2 concentration, and birnessite dose (HA_b) was used for later characterization, soil sedimentation, and wheat seed germination experiments. For comparison purpose, HA was also extracted using the IHSS method (HA_I), with danty crushed for the same time.

2.4. HA Characterization. *2.4.1. Fourier Transform Infrared (FTIR) Spectroscopy.* To identify the functional groups of danty, HA_c, HA_I, and HA_b, approximately 0.5 mg of dried sample was ground with 100 mg KBr and compacted to form pellets. FTIR spectra were recorded between 400 and 4000 cm^{-1} at a resolution of 4 cm^{-1} using an FTIR spectrometer (TENSOR 27, Bruker Co., Germany).

2.4.2. Acidic Functional Group Titration. The content of acidic functional groups was measured based on the amount of $BaCl_2$ adsorbed by the acidic functional groups.[22] The content of −COOH groups was determined by potentiometric titration of the acetic acid released from the reaction with calcium acetate. The content of phenolic −OH was calculated as the difference between total acidity and −COOH content.

2.4.3. UV−vis Spectroscopy. The danty, HA_c, HA_I, and HA_b were dissolved in 0.05 mol L^{-1} $NaHCO_3$. The absorbances at 465 nm (E_{465}) and 665 nm (E_{665}) were determined using a UV−vis spectrophotometer (T6 New Century, China), and E_{465}/E_{665} ratio was calculated.[25]

2.4.4. Electrospray Ionization Fourier Transform Ion Cyclotron Resonance Mass Spectrometry (ESI-FT-ICR-MS). Before ESI-FT-ICR-MS analysis, the purified danty and HA_b were purified according to the procedure described by Melendez-Perez et al.,[26] dissolved in NH_3 solution (10%, analytical grade), and passed through a column packed with protonated cation exchange resin (Agilent, USA, Bond Elut-PPL, 1 g 6 mL, 30/PK).[27] Then, ultrahigh-resolution mass spectra were obtained using a SolariX XR mass spectrometer (Bruker Daltonics, USA) equipped with a 9.4 T superconducting magnet and a dual-mode ESI/MALDI ion source.[26−28]

2.4.5. HA Flocculation Test. In tubes containing 5 mL 0.02 wt % HA_c, HA_b, and HA_I solutions, different volumes (in

https://doi.org/10.1021/acsomega.2c06411
ACS Omega 2022, 7, 47192−47201

increments of no more than 0.02 mL) of 0.1 mol L^{-1} $CaCl_2$ and $MgSO_4$ solutions were added. Then, about 15 mL of deionized water was added and the pH was adjusted to maintain the pH between 8.0 and 8.5 in each tube. Finally, the volume was fixed to 25 mL with deionized water. The tubes were shaken, left to stand for approximately an hour, and observed for the occurrence of flocculation. The flocculation limit (C_{max}, mmol mL^{-1}) was calculated as follows (eq 1):

$$C_{max} = \frac{M \times V \times 1000}{5} \quad (1)$$

where M is the concentration of $CaCl_2$ solution added (i.e., 0.1 mol L^{-1}), and V is the minimum volume of $CaCl_2$ solution added for the occurrence of flocculation (mL).

2.5. Application HA. *2.5.1. Sedimentation Experiment.* In 50 mL plastic centrifuge tubes containing 0.14 g of danty, HA_c, HA_b, and HA_I, 10 g calcareous soil, and 25 mL of deionized water were added. After shaking with water for 10 min, centrifuged the supernatant to determine the relevant indices, and then re-added water for extraction, and repeated the above operation four times. The soil−danty/HA systems was measured for absorbance at 665 nm after 0.5, 1, 2, 3.5, 15.5, and 36 h using a UV−vis spectrophotometer (T6 new century, China). Zeta potential of the soil−danty/HA systems was measured using a laser particle size analyzer (Zetasizer Nano S, Malvern, UK). For determination of CO_3^{2-} and HCO_3^- contents, 10 mL supernatant with phenolphthalein indicator added was titrated with the standard sulfuric acid solution (V_1) until colorless. After the bromophenol blue indicator was added, the supernatant was titrated with the standard sulfuric acid solution (V_2) again until colorless. The contents of CO_3^{2-} (C_1, g kg^{-1}) and HCO_3^- (C_2, g kg^{-1}) were calculated as follows (eqs 2, 3):

$$C_1 = \frac{2V_1 \times c \times 10 \times 3}{25 \times 10} \quad (2)$$

$$C_2 = \frac{(V_2 - 2V_1) \times c \times 10 \times 6.1}{25 \times 10} \quad (3)$$

where c is the concentration of the standard sulfuric acid solution (mol L^{-1}).

2.5.2. Seed Germination Experiment. In this experiment, the germination of wheat seeds was tested in two media: $NaHCO_3$ (i.e., alkaline stress; pH = 8.41) and NaCl (i.e., salt stress; pH = 6.83). For calcareous soil buffering effect to pH changes brought on by the addition of acid or alkali, calcareous soil relies on CO_3^{2-}/HCO_3^-, so $NaHCO_3$ was used to simulate the alkaline stress environment to make the environment more suitable for the calcareous soil itself. For the two media, the concentration of NaCl and $NaHCO_3$ were both 0.1 mol L^{-1}. The aqueous solutions of five samples, including CK (deionized water), danty (1 g L^{-1}), HA_c (1 g L^{-1}), HA_b (1 g L^{-1}), and HA_I (1 g L^{-1}), were added to the two media, respectively. Thirty-six wheat seeds were grown in each medium (6 × 6) with 9 replicates per treatment. The seeds were then placed in an incubator under constant growing conditions of 25 °C and humidity of 50−60%. After 24 and 48 h, the number of germinated seeds was recorded, and the germination rate was calculated.

3. RESULTS AND DISCUSSION

3.1. Morphological, Structural, and Chemical Properties of the Prepared Birnessite. The crystal structure of the prepared birnessite was analyzed using XRD (Figure 1A). The

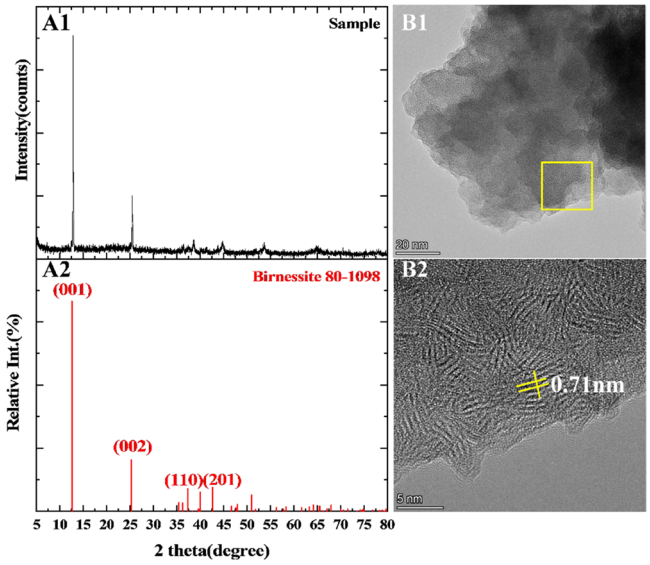

Figure 1. X-ray diffraction patterns of (A1) prepared birnessite and (A2) standard birnessite; transmission electron microscopy images of (B1 and B2) prepared birnessite.

intense diffraction peaks of 2θ located at approximately 12.9° (001), 25.7° (002), 36.4° (110), and 40.2° (201) can be assigned to the hexagonal phase (JCPDS no. 80-1098) of the birnessite structure.[29,30] It can be seen from the XRD pattern that the crystallinity was good. Therefore, the structure of manganese oxide was ascribed to birnessite with a certain extent of the amorphous state. The interlayer distance (d) was calculated according to Bragg's law: $2d\sin\theta = \lambda$, where θ is the Bragg angle, and λ is the X-ray wavelength. The diffraction peak at 12.9° assigned to {001} facet was used to calculate the lattice distance, and the calculated result (0.71 nm) was consistent with that observed by TEM (Figure 1B).[30] The results indicate that typical birnessite was synthesized and no additional crystalline phase was formed.

The catalytic activity of birnessite depends on the average valence of manganese. The XPS Mn 2p spectrum of the prepared birnessite displayed two peaks at 642.3 and 654.1 eV, which were assigned to Mn $2p_{3/2}$ and Mn $2p_{1/2}$, respectively (Figure 2A). The Mn $2p_{3/2}$ peak can be deconvoluted into three peaks at 640.7−640.8, 643.5−643.6, and 642.1−642.3 eV, which were assigned to Mn^{2+}, Mn^{3+}, and Mn^{4+}, respectively.[20,29] After curve-fitting, the ratio between Mn^{4+} species (642.9 ± 0.1 eV) and Mn^{3+} species (641.6 ± 0.1 eV) was calculated to be 33.95%, and the binding energy difference (E) of Mn 3s was 4.8 eV (Figure S3). As the average oxidation state (AOS) of manganese is calculated as 8.956−1.126E, the AOS of manganese in the prepared birnessite was 3.55, indicating that manganese can undergo both oxidation and reduction reactions to facilitate electron transfer in the prepared birnessite.

The XPS O 1s spectrum of the prepared birnessite is shown in Figure 2B. The peaks at approximately 529.7−529.8, 530.5−530.8, and 532.9−533.5 eV corresponded to lattice oxygen (O_{latt}), surface adsorbed oxygen (O_{surf}), and surface residual water, respectively. Surface-adsorbed oxygen readily participates in oxidation reactions due to its high activity.[31] The surface-adsorbed oxygen took up 51.6% of the total oxygen in the prepared birnessite, which indicates that the prepared birnessite was redox-active.

https://doi.org/10.1021/acsomega.2c06411
ACS Omega 2022, 7, 47192−47201

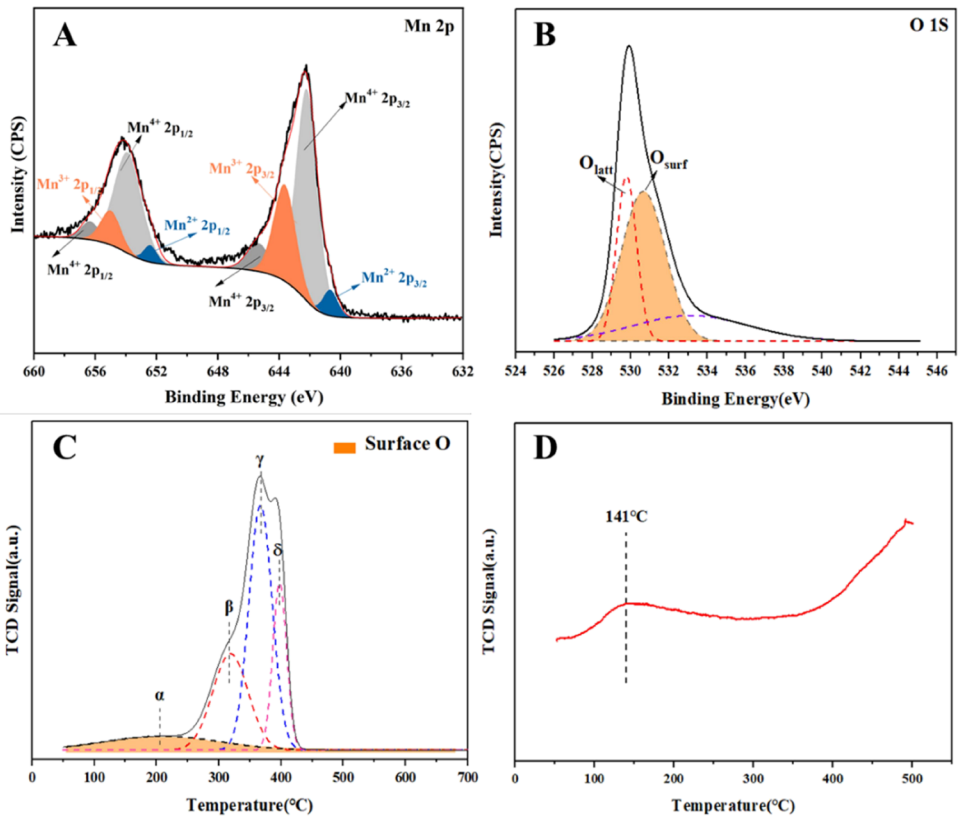

Figure 2. X-ray photoelectron spectroscopy (XPS) spectra of (A) Mn 2p and (B) O 1s, (C) hydrogen temperature-programmed reduction (H_2-TPR) profile, and (D) oxygen temperature-programmed desorption (O_2-TPD) profile of the prepared birnessite.

The reducibility of the prepared birnessite was evaluated by H_2-TPR. As shown in Figure 2C, the TPR profile of the prepared birnessite can be divided into peaks α, β, γ, and δ. The reduction temperature of peak α was 205.3 °C, and the initial reduction temperature of lattice oxygen represented by peak β was 316.2 °C.[32] Representing the consumption of surface-adsorbed oxygen species, peak α was the desorption peak of surface chemisorbed oxygen (O_2^-, O^-, etc.), and the surface adsorbed oxygen could be converted to surface lattice oxygen. Peak β, γ, and δ, with a peak area ratio of about 1:2:1, represented the successive reductions of $K_xMnO_2 \rightarrow Mn_2O_3 \rightarrow Mn_3O_4 \rightarrow MnO$.[32,33] In addition, O_2-TPD was used to characterize the oxygen desorption performance of the catalyst (Figure 2D), and the result showed that the desorption peak of surface chemisorbed oxygen was at 141 °C, indicating that the prepared birnessite was a strong oxidant. The temperature (60 °C) during HA extraction in this study was below 141 °C (Figure 2B). Therefore, the birnessite was active during the whole reaction process.

3.2. Optimization of HA Extraction Condition. The acidic functional groups such as phenolic hydroxyl and carboxyl play a crucial role in HA quality. The results of single-factor experiments showed that the acidic functional group content of the extracted HA was significantly affected by birnessite dose, H_2O_2 concentration, and danty crushing time (Figure 3A–C). Acidic functional group content increased with increasing H_2O_2 concentration from 0.5 to 20% (Figure 3B) but did not change significantly when H_2O_2 concentration increased from 20 to 25%. It first increased and then decreased with increasing birnessite dose, peaking at approximately 1.5% (Figure 3A). Similarly, it first increased and then decreased with danty crushing time, peaking around 100 min (Figure 3C).

The RSM was used to determine the optimal combination of (A) birnessite dose, (B) H_2O_2 concentration, and (C) danty crushing time for maximum content of acidic functional groups of the extracted HA. Birnessite dose, H_2O_2 concentration, and danty crushing time were set at 1–2%, 20–25%, and 90–120 min, respectively, based on the results of single-factor experiments (Figure 3A–C).

The model of the correlation between HA acidic functional group content (Y) and (A) birnessite dose, (B) H_2O_2 concentration, and (C) danty crushing time was obtained using Design-Expert software (Figure 3D–F). The fitting results according eq 4 showed that at birnessite dose of 2.0%, H_2O_2 concentration at 20%, and danty crushing time of 105.7 min, the content of acidic functional groups of the extracted HA (HA_b) was the highest, 84.3, 102.3, and 115.2% higher than that of HA_I, HA_c, and danty, respectively.

The Prob > F value of the model was 0.0017 ($P < 0.05$), indicating that the response surface regression model was significant with a good fit to the data. The coefficient of determination (R^2) was 99.09%, indicating that the regression model can well explain the variation in acidic functional group content.[24]

https://doi.org/10.1021/acsomega.2c06411
ACS Omega 2022, 7, 47192–47201

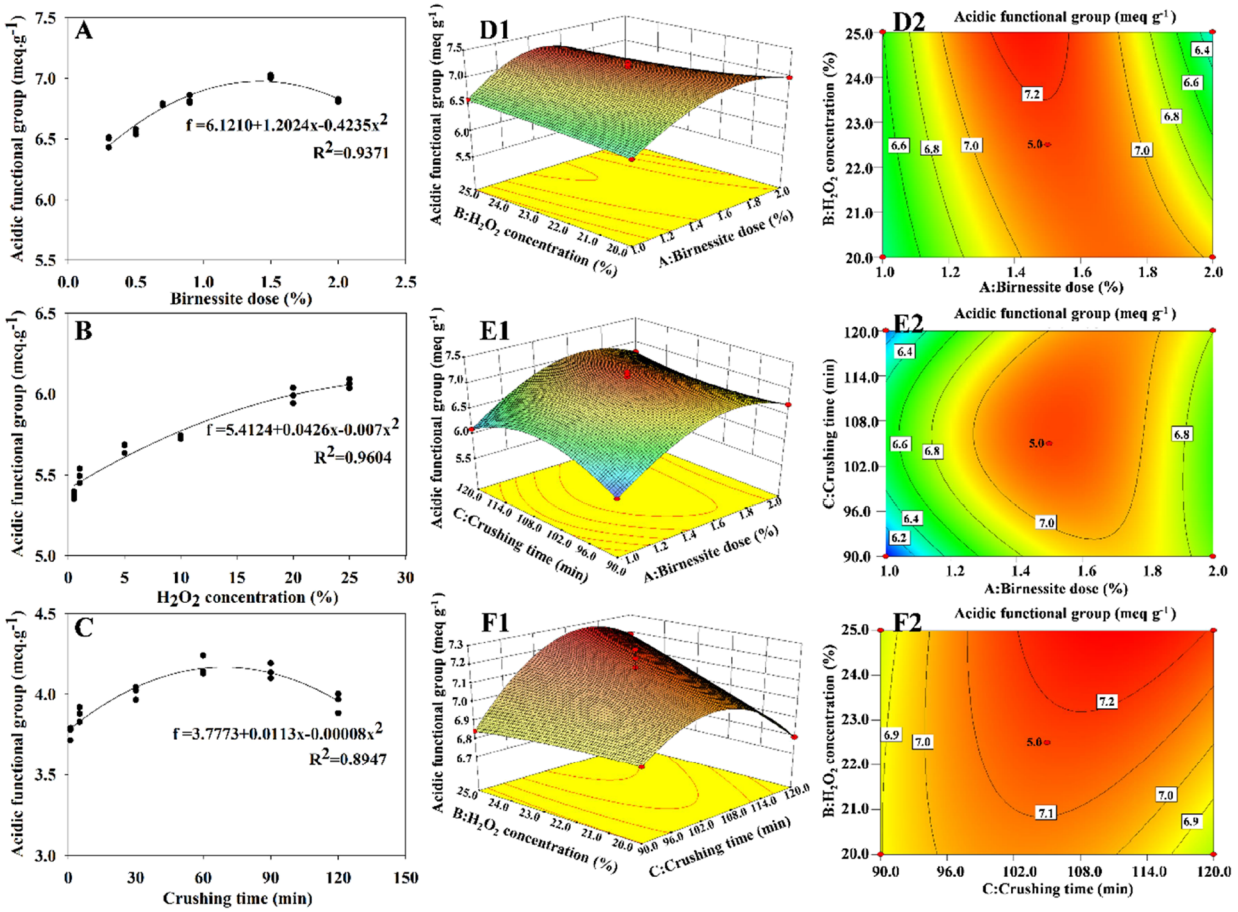

Figure 3. Plots of the relationships between (A) birnessite dose, (B) H_2O_2 concentration, and (C) danty crushing time and acidic functional group content of the extracted HA. Three-dimensional plots and contour maps showing the effects of the interactions between A and B (D1 and D2), A and C (E1 and E2), and B and C (F1 and F2) on the acidic functional group content of extracted HA.

$$Y = 0.14 - 1.385 \times 10^{-3}A - 1.222 \times 10^{-3}B - 1.747 \times 10^{-3}C + 2.838 \times 10^{-4}AB + 5.076 \times 10^{-3}AC - 2.308 \times 10^{-3}BC + 0.013A^2 + 4.492 \times 10^{-3}B^2 + 3.389 \times 10^{-4}C^2 - 9.233 \times 10^{-5}A^2B + 4.462 \times 10^{-3}A^2C - 7.357 \times 10^{-3}AB^2 \quad (4)$$

3.3. HA Characterization. The FTIR spectra of danty, HA_c, HA_I, and HA_b are shown in Figure 4. The peak at 1708 cm^{-1}, which corresponded to the stretching vibration of C═O in carboxyl or keto groups,[34] appeared in all four spectra but showed a much higher intensity in the spectrum of HA_b than in the other spectra. The peaks at 3420 and 1601 cm^{-1} were attributed to the O−H and C═C bonds in aromatic rings, respectively.[35] The peak at 1094 cm^{-1} in the spectrum of danty was due to aliphatic alcohol, ether, or thiol groups, but it was not observed in the spectra of HA_b and HA_c. Though the spectra of HA_I and HA_b displayed almost the same peaks, the peaks in the spectrum of HA_b were of much higher intensity, indicating that HA_b had more surface functional groups.

The contents of acidic functional groups, −COOH group, and phenolic −OH group and the E_{465}/E_{665} ratios of danty, HA_c, HA_b, and HA_I are summarized in Table 1. Carboxyl and phenolic hydroxyl groups make up the acidic functional groups of HA. The higher its acidic functional group content, the more chemically active the HA.[36] The acidic functional group

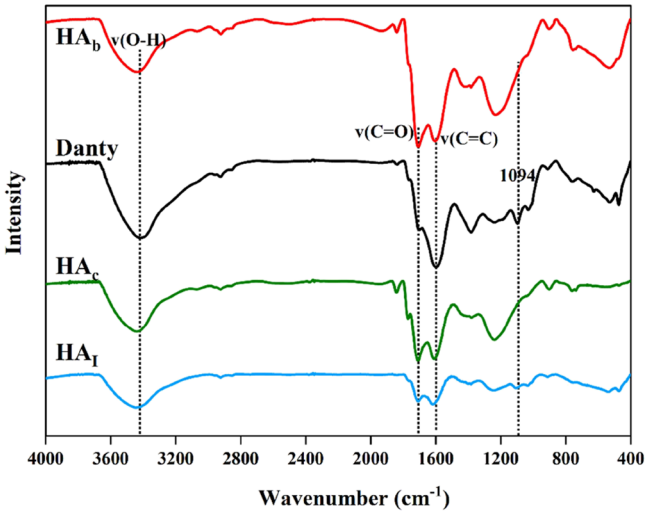

Figure 4. Fourier transform infrared spectra of the danty used for humic acid extraction (Danty), commercial humic acid (HA_c), humic acid extracted using the International Humic Substances Society method (HA_I), and humic acid extracted using the catalytic oxidation method of this study under optimal conditions (HA_b).

contents were 7.06, 3.49, and 3.83 meq g^{-1}, the −COOH group contents were 6.61, 2.84, and 3.02 meq g^{-1}, and the phenolic −OH group contents were 0.45, 0.65, and 0.81 meq g^{-1}

https://doi.org/10.1021/acsomega.2c06411
ACS Omega 2022, 7, 47192−47201

Table 1. Acidic Functional Group, Carboxyl Group, and Phenolic Hydroxyl Group Contents, E_{465}/E_{665} Ratios, and Flocculation Limits of the Danty Used for Humic Acid Extraction, Commercial Humic Acid (HA_c), Humic Acid Extracted Using the International Humic Substances Society Method (HA_I), and Humic Acid Extracted Using the Catalytic Oxidation Method of this Study under Optimal Conditions (HA_b)

property	component	danty	HA_c	HA_I	HA_b
functional group (meq g^{-1})	acidic functional group	3.28	3.49	3.83	7.06
	carboxylic	0.91	2.84	3.02	6.61
	phenolic	2.37	0.65	0.81	0.45
UV−vis analysis	E_{465}	0.22	1.42	2.63	2.40
	E_{665}	0.08	0.43	0.55	0.54
	E_{465}/E_{665} ratio	2.59	3.29	4.31	4.40
flocculation limit (mmol L^{-1})	$CaCl_2$		2.8	2.8	5.6
	$MgSO_4$		36.0	40.0	48.0

in HA_b, HA_c, and HA_I, respectively. Compared with the danty, HA_b had higher contents of acidic and -COOH groups. Compared with HA_I, the acidic functional group content of HA_b increased by 84.3%, which was due to catalytic oxidation.

It is commonly known that the E_{465}/E_{665} ratio of HA is correlated with its average molecular weight and size and oxygen content. In addition, E_{465}/E_{665} ratio decreases with an increase in the condensation of HA. As shown in Table 1, the E_{465}/E_{665} ratios of danty, HA_c, HA_I, and HA_b were lower than 5, displaying a typical UV−vis property of HA. The E_{465}/E_{665} ratio of HA_b (4.40) was higher than those of HA_c (3.29) and HA_I (4.31), indicating that HA_b had a lower average molecular weight and a higher oxygen content than HA_c and HA_I. The flocculation limits of HA_b, HA_c, and HA_I were 5.6, 2.8, and 2.8 mmol L^{-1}, respectively, in $CaCl_2$ solution and 48.0, 36.0, and 40.0 mmol L^{-1}, respectively, in $MgSO_4$ solution (Table 1). The higher flocculation limit values of HA_b may be related to the lower molecular weight caused by catalytic oxidation.

ESI-FT-ICR-MS is a powerful structural analysis technology. It is widely employed to distinguish substances of similar sources. The Van Krevelen diagrams illustrate the molecular compositions of HA_b (Figure 5A) and the danty (Figure 5B). According to the H/C and O/C ratios, the HA_b and danty were composed of the following seven groups of components: lipid-like (H/C: 1.5−2.0; O/C: 0−0.3), protein-like (H/C: 1.5−2.2; O/C: 0.3−0.67), carbohydrate-like (H/C: 1.5−2.2; O/C: 0.67−1.2), unsaturated hydrocarbon-like (H/C: 0.7−1.5; O/C: 0−0.1), lignin-like (H/C: 0.7−1.5; O/C: 0.1−0.67), tannin-like (H/C: 0−1.5; O/C: 0.67−1.2), and condensed aromatic component (H/C: 0.2−0.7; O/C: 0−0.67) (Figure 5C).[26,27,37] Compared with the danty, HA_b extracted via catalytic oxidation showed significantly lower relative abundances of lipid, protein, unsaturated hydrocarbon, and lignin (Figure 5A,B). For instance, lipid and protein relative abundances in the danty were 4.2 and 0.15%, compared to 0.5 and 0.03% in the HA_b. The relative abundance of unsaturated hydrocarbons in the danty was 0.2%, which was 10 times that of HA_b (Figure 5D). Additionally, the content of lignin in HA_b was reduced by 67.2%

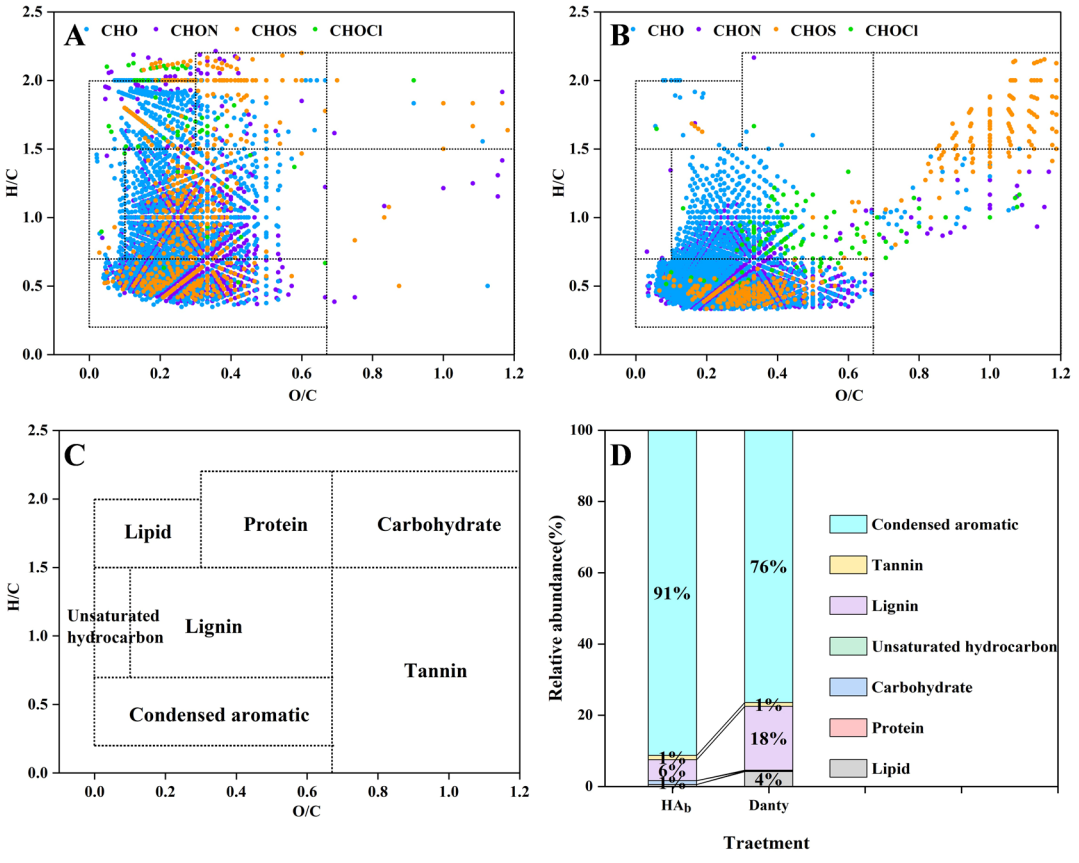

Figure 5. Van Krevelen diagrams of (A) humic acid extracted from danty via catalytic oxidation under optimal conditions (HA_b), (B) danty used for HA_b extraction, (C) humic acid component classification based on H/C and O/C ratios, and (D) component relative abundances of the danty and HA_b.

https://doi.org/10.1021/acsomega.2c06411
ACS Omega 2022, 7, 47192−47201

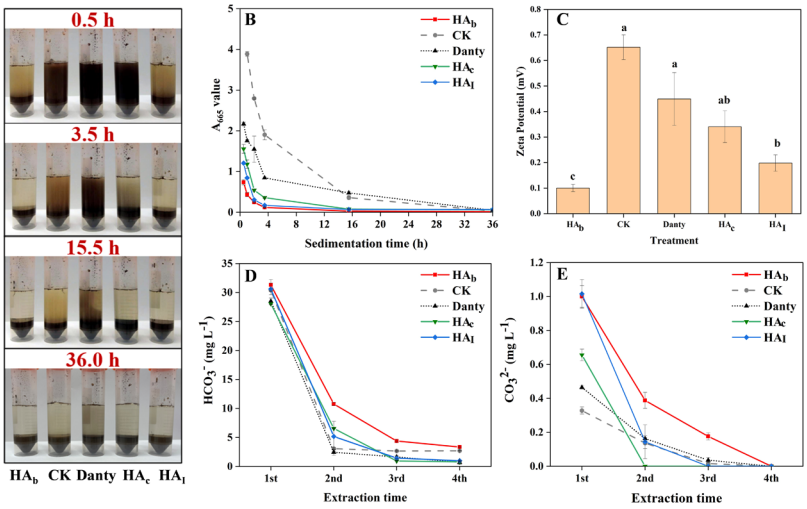

Figure 6. (A) Photos showing soil sedimentation processes in tubes with addition of humic acid extracted using the catalytic oxidation method of this study under optimal conditions (HA_b), no danty or humic acid (CK), the danty used for humic acid extraction (Danty), commercial humic acid (HA_c), and humic acid extracted using the International Humic Substances Society method (HA_I); (B) changes in supernatant absorbance at 665 nm (A_{665}) during soil sedimentation in the tubes; (C) zeta potentials of soil−danty/HA systems; (D) HCO_3^- content changes with four-time extraction; and (E) CO_3^{2-} content changes with four-time extraction.

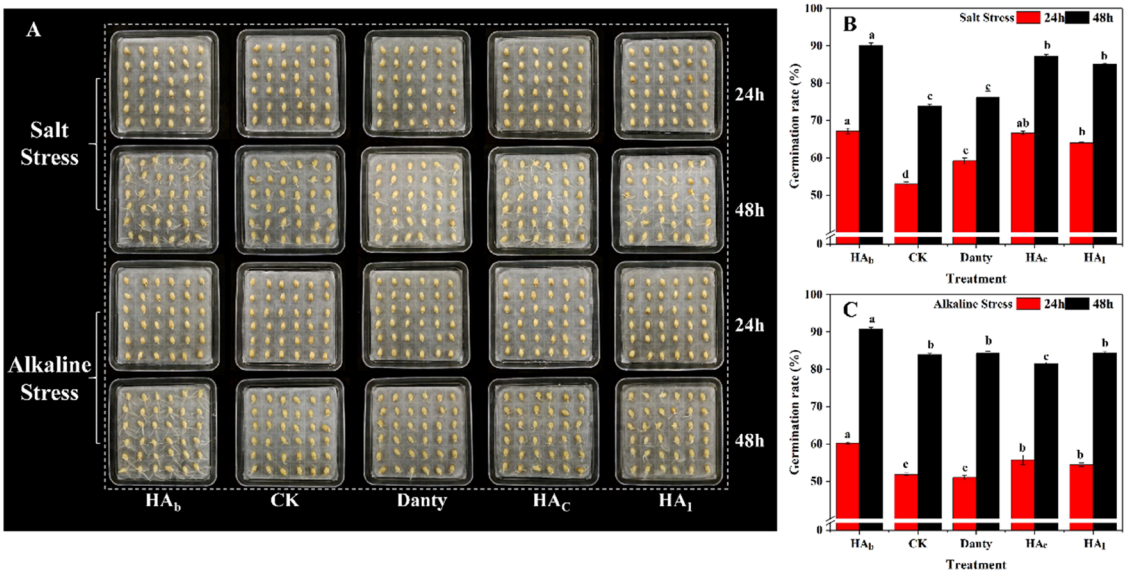

Figure 7. (A) Photos showing seeds germinated under salt and alkaline stress; (B) germination rates of wheat seeds in NaCl solution (i.e., salt stress) and (C) $NaHCO_3$ solution (i.e., alkaline stress).

compared with danty (Table S3). In contrast, the relative abundances of carbohydrate and condensed aromatic were higher in HA_b than in the danty. For example, the relative abundance of carbohydrate was 0.04% in the danty, and it was 1.1% in HA_b. This may be related to the significant increase in the content of functional groups such as carboxyl groups in HA_b (Table 1). The increase of condensed aromatics and reaction speed in HA_b indicated that side chains between the molecule and the hydrogen of the aromatic ring were decreased (Figure S4). This could be caused by aromatic ring molecules being linked to each other by acidic functional groups during catalytic oxidation.[3,23,37]

3.4. Beneficial Effects of HA on Soil and Plant. Figure 6A shows the sedimentation process of the calcareous soil with addition of the A shows the sedimentation process of the calcareous soil with the addition of different samples$_b$, CK and danty, HA_c, and HA_I. After 0.5-h standing, the supernatants in the tubes with HA_b and HA_I added were much clearer than those in the other tubes. After 3.5 h, most of the soil particles in the tube with HA_c added had settled down in the bottom of the tube, whereas almost all soil particles in the tubes with HA_b and HA_I had settled down in the bottom. In contrast, many particles in the tube with no danty or HA added (CK) were still suspended, and very few in the tube with the danty added had settled down. Only after 36 h, clear supernatants were observed in CK and the tube with danty. Soil settlement is affected by soil properties like particle size, organic matter content, pH value, and so on. According to Stokes' law, the settlement rate of soil particles is determined by the colloidal dispersion system.[38] It can be seen in Figure 6B that the A_{665} values of the supernatants in the tubes with HA added decreased much more rapidly than those in CK and the tube with danty added. As for the three HA treatments,

https://doi.org/10.1021/acsomega.2c06411
ACS Omega 2022, 7, 47192−47201

A_{665} decreased most rapidly in HA_b, followed by HA_I and then HA_c. Figure 6A,B demonstrates that HA can accelerate the sedimentation of calcareous soil, which may be related to its acidic functional groups of −COOH and phenol −OH.[25] Figure 6C shows that zeta potential was significantly lower in the HA_b and HA_I treatments than in CK and the danty treatment. This could be explained by the deprotonation of the −OH/−COOH groups, which generated H^+ ions to react with the OH^- ions. As a result, the electrostatic double layers became thinner, and zeta potential decreased. As HA_b and HA_I possessed more −OH/−COOH groups (Table 1),[39] their addition to the calcareous alkaline soil led to larger decreases in zeta potential. It could be explained that adding HA changed the original properties of the colloidal dispersion system due to the action of acid functional groups, thereby accelerating calcareous soil settlement.[38]

Calcareous soils have a poor structure because of their high contents of calcium carbonate and magnesium carbonate, which are sparsely soluble. The concentrations of HCO_3^- and CO_3^{2-} in the extract were always higher in the HA_b treatment than in the other treatments (Figure 6D,E), indicating that HA_b performed better in promoting the continuous dissolution of calcium carbonate and magnesium carbonate from the calcareous soil, which would lead to a better structure and quality of calcareous soils. For soil buffering effect to pH changes brought on by the addition of acid or alkali, calcareous soil rely on sodium bicarbonate. The effect of HA on the acid−base buffer system (HCO_3^-/CO_3^{2-}) can also be used to adjust the pH of calcareous soil.

Wheat seeds under saline and alkaline stress were shown in terms of their growth status (Figure 7A) and germination rate (Figure 7B,C). In the salt stress environment, application of HA increased the germination percentage of wheat seeds by 15.2−21.9%, and HA_b treatment had the best effect. Under alkaline stress conditions, application of HA promoted wheat germination significantly in the first 24 h.[6] After 48 h, the effect of danty and HA_I samples was not statistically different from CK in germination rate, but HA_b was still significantly better than CK. These findings indicated that HA_b extracted via catalytic oxidation had a significant promotion effect on wheat seed germination percentage in a saline−alkaline stress environment.[40] This could be attributed to the highlong-term performance of the acidic functional groups (Table 1) and organic matter components (Figure 5A,B).[41,42]

4. CONCLUSIONS

Birnessite with good crystallinity was prepared in this study. The lattice contained active oxygen, and with an AOS of 3.55, manganese had a good catalytic ability. The prepared birnessite was applied as a catalyst in the extraction of HA from danty, and the obtained HA had high contents of acidic functional groups. Extraction conditions were optimized using single-factor experiments and RSM. The optimal HA extraction conditions were found to be danty crushing time of 105.7 min, H_2O_2 concentration of 20.0%, and birnessite dose of 2.0%. The HA extracted via catalytic oxidation under optimal conditions performed better than commercial HA and that extracted using the conventional IHSS method in promoting the aggregation of calcareous soil. The HA sample extracted by catalytic oxidation could improve the growth of wheat seeds under saline and alkaline stress conditions, and it could be applied in calcareous soils to improve the soil structure by promoting aggregation, as well as crop growth and agricultural production.

ASSOCIATED CONTENT

Supporting Information

The Supporting Information is available free of charge at https://pubs.acs.org/doi/10.1021/acsomega.2c06411.

Pictures of humic acid taken both before and after washing; pH value and the intensity of the H, Cl element of HA samples; XPS-Mn 3s analysis of birnessite sample; plot of acidic functional group content as a function of catalytic oxidation time; single-factor design for optimal conditions of humic acid extraction; parameters of the three-factor surface response model; and component relative abundances (%) of the danty and HA_b (PDF)

AUTHOR INFORMATION

Corresponding Authors

Qi Chen − *National Engineering Research Center for Efficient Utilization of Soil and Fertilizer Resources, College of Resources and Environment, Shandong Agricultural University, Tai an, Shandong 271018, China*; Email: chenqi_sdau@163.com

Jibiao Geng − *College of Resources and Environment, Linyi University, Linyi, Shandong 276000, China*; Email: gengjibiao@126.com

Authors

Zixin Zhang − *National Engineering Research Center for Efficient Utilization of Soil and Fertilizer Resources, College of Resources and Environment, Shandong Agricultural University, Tai an, Shandong 271018, China*

Guohua Ma − *National Engineering Research Center for Efficient Utilization of Soil and Fertilizer Resources, College of Resources and Environment, Shandong Agricultural University, Tai an, Shandong 271018, China*

Kexin Zhang − *National Engineering Research Center for Efficient Utilization of Soil and Fertilizer Resources, College of Resources and Environment, Shandong Agricultural University, Tai an, Shandong 271018, China*

Zhaoming Qu − *National Engineering Research Center for Efficient Utilization of Soil and Fertilizer Resources, College of Resources and Environment, Shandong Agricultural University, Tai an, Shandong 271018, China*

Gaoyang E − *National Engineering Research Center for Efficient Utilization of Soil and Fertilizer Resources, College of Resources and Environment, Shandong Agricultural University, Tai an, Shandong 271018, China*

Conghui Wang − *National Engineering Research Center for Efficient Utilization of Soil and Fertilizer Resources, College of Resources and Environment, Shandong Agricultural University, Tai an, Shandong 271018, China*

Peng Zhang − *Shandong Wanhao Fertilizer Co., Jinan 251600, China*

Zhiguang Liu − *National Engineering Research Center for Efficient Utilization of Soil and Fertilizer Resources, College of Resources and Environment, Shandong Agricultural University, Tai an, Shandong 271018, China*; orcid.org/0000-0002-8844-1112

Min Zhang − *National Engineering Research Center for Efficient Utilization of Soil and Fertilizer Resources, College of Resources and Environment, Shandong Agricultural University, Tai an, Shandong 271018, China*; orcid.org/0000-0002-7838-3393

Complete contact information is available at:

https://doi.org/10.1021/acsomega.2c06411
ACS Omega 2022, 7, 47192−47201

https://pubs.acs.org/10.1021/acsomega.2c06411

Notes

The authors declare no competing financial interest.

■ ACKNOWLEDGMENTS

This work was supported by the National Natural Science Foundation of China (Grant nos. 42277356, 41977019, and CX41907067) and the Agricultural application technology innovation project (Grant no. CX202215).

■ REFERENCES

(1) Bleam, W.Chapter 7 − Natural Organic Matter. In *Soil and Environmental Chemistry*, 2nd ed.; Bleam, W. Ed.; Academic Press, 2017; pp 333−384.

(2) Yang, Z.; Kappler, A.; Jiang, J. Reducing Capacities and Distribution of Redox-Active Functional Groups in Low Molecular Weight Fractions of Humic Acids. *Environ. Sci. Technol.* **2016**, *50*, 12105−12113.

(3) de Melo, B. A.; Motta, F. L.; Santana, M. H. Humic acids: Structural properties and multiple functionalities for novel technological developments. *Mater. Sci. Eng. C* **2016**, *62*, 967−974.

(4) Han, Y.-N.; Bai, Z.-Q.; Liao, J.-J.; Bai, J.; Dai, X.; Li, X.; Xu, J.-L.; Li, W. Effects of phenolic hydroxyl and carboxyl groups on the concentration of different forms of water in brown coal and their dewatering energy. *Fuel Process. Technol.* **2016**, *154*, 7−18.

(5) Xiong, L.; Wang, P.; Hunter, M. N.; Kopittke, P. M. Bioavailability and movement of hydroxyapatite nanoparticles (HA-NPs) applied as a phosphorus fertiliser in soils. *Environ. Sci.: Nano* **2018**, *5*, 2888−2898.

(6) Chen, Q.; Qu, Z.; Ma, G.; Wang, W.; Dai, J.; Zhang, M.; Wei, Z.; Liu, Z. Humic acid modulates growth, photosynthesis, hormone and osmolytes system of maize under drought conditions. *Agric. Water Manage.* **2022**, *263*, No. 107447.

(7) Canellas, L. P.; Olivares, F. L.; Aguiar, N. O.; Jones, D. L.; Nebbioso, A.; Mazzei, P.; Piccolo, A. Humic and fulvic acids as biostimulants in horticulture. *Sci. Hortic.* **2015**, *196*, 15−27.

(8) Cooke, J. D.; Hamilton-Taylor, J.; Tipping, E. On the Acid−Base Properties of Humic Acid in Soil. *Environ. Sci. Technol.* **2007**, *41*, 465−470.

(9) Perdue, E. M.Standard and Reference Samples of Humic Acids, Fulvic Acids, and Natural Organic Matter from the Suwannee River, Georgia: Thirty Years of Isolation and Characterization. In *Functions of Natural Organic Matter in Changing Environment*; Xu, J., Wu, J., He, Y., Eds.; Springer Netherlands: Dordrecht, 2013; pp 85−88.

(10) Zhang, J.; Chen, L.; Yin, H.; Jin, S.; Liu, F.; Chen, H. Mechanism study of humic acid functional groups for Cr(VI) retention: Two-dimensional FTIR and (13)C CP/MAS NMR correlation spectroscopic analysis. *Environ. Pollut.* **2017**, *225*, 86−92.

(11) Ritchie, J. D.; Perdue, E. M. Analytical constraints on acidic functional groups in humic substances. *Org. Geochem.* **2008**, *39*, 783−799.

(12) Tang, Y.; Yang, Y.; Dongdong, C.; Gao, B.; Wan, Y.; Yao, Y.; Xie, J.; Liu, L. Multifunctional Slow-Release Fertilizer Prepared from Lignite Activated by a 3D-Molybdate-Sulfur Hierarchical Hollow Nanosphere Catalyst. *ACS Sustainable Chem. Eng.* **2019**, *7*, 10533−10543.

(13) Sarlaki, E.; Sharif Paghaleh, A.; Kianmehr, M. H.; Asefpour Vakilian, K. Extraction and purification of humic acids from lignite wastes using alkaline treatment and membrane ultrafiltration. *J. Cleaner Prod.* **2019**, *235*, 712−723.

(14) Zhou, H.; Zhu, X.; Chen, B. Magnetic biochar supported alpha-MnO_2 nanorod for adsorption enhanced degradation of 4-chlorophenol via activation of peroxydisulfate. *Sci. Total Environ.* **2020**, *724*, No. 138278.

(15) Hao, J.; Meng, X.; Fang, S.; Cao, H.; Lv, W.; Zheng, X.; Liu, C.; Chen, M.; Sun, Z. MnO_2-Functionalized Amorphous Carbon Sorbents from Spent Lithium-Ion Batteries for Highly Efficient Removal of Cadmium from Aqueous Solutions. *Ind. Eng. Chem. Res.* **2020**, *59*, 10210−10220.

(16) Boyom-Tatchemo, F. W.; Devred, F.; Ndiffo-Yemeli, G.; Laminsi, S.; Gaigneaux, E. M. Plasma-induced redox reactions synthesis of nanosized α-, γ- and δ-MnO_2 catalysts for dye degradation. *Appl. Catal., B* **2020**, *260*, No. 118159.

(17) Balakumar, V.; Ryu, J. W.; Kim, H.; Manivannan, R.; Son, Y. A. Ultrasonic synthesis of alpha-MnO_2 nanorods: An efficient catalytic conversion of refractory pollutant, methylene blue. *Ultrason. Sonochem.* **2020**, *62*, No. 104870.

(18) Xia, D.; Liu, H.; Xu, B.; Wang, Y.; Liao, Y.; Huang, Y.; Ye, L.; He, C.; Wong, P. K.; Qiu, R. Single Ag atom engineered 3D-MnO_2 porous hollow microspheres for rapid photothermocatalytic inactivation of E. coli under solar light. *Appl. Catal., B* **2019**, *245*, 177−189.

(19) Wu, B.; Li, Y.; Su, K.; Tan, L.; Liu, X.; Cui, Z.; Yang, X.; Liang, Y.; Li, Z.; Zhu, S.; et al. The enhanced photocatalytic properties of MnO_2/g-C_3N_4 heterostructure for rapid sterilization under visible light. *J. Hazard. Mater.* **2019**, *377*, 227−236.

(20) Zhu, L.; Wang, J.; Rong, S.; Wang, H.; Zhang, P. Cerium modified birnessite-type MnO_2 for gaseous formaldehyde oxidation at low temperature. *Appl. Catal., B* **2017**, *211*, 212−221.

(21) Doskočil, L.; Burdíková-Szewieczková, J.; Enev, V.; Kalina, L.; Wasserbauer, J. Spectral characterization and comparison of humic acids isolated from some European lignites. *Fuel* **2018**, *213*, 123−132.

(22) Sarlaki, E.; Sharif Paghaleh, A.; Kianmehr, M. H.; Asefpour Vakilian, K. Valorization of lignite wastes into humic acids: Process optimization, energy efficiency and structural features analysis. *Renewable Energy* **2021**, *163*, 105−122.

(23) Fatima, N.; Jamal, A.; Huang, Z.; Liaquat, R.; Ahmad, B.; Haider, R.; Ali, M. I.; Shoukat, T.; Alothman, Z. A.; Ouladsmane, M.; Ali, T.; Ali, S.; Akhtar, N.; Sillanpä, M. Extraction and Chemical Characterization of Humic Acid from Nitric Acid Treated Lignite and Bituminous Coal Samples. *Sustainability* **2021**, *13*, 2071−1050.

(24) Tian, H.; Liu, Z.; Zhang, M.; Guo, Y.; Zheng, L.; Li, Y. C. Biobased Polyurethane, Epoxy Resin, and Polyolefin Wax Composite Coating for Controlled-Release Fertilizer. *ACS Appl. Mater.* **2019**, *11*, 5380−5392.

(25) Dos Santos, J. V.; Fregolente, L. G.; Moreira, A. B.; Ferreira, O. P.; Mounier, S.; Viguier, B.; Hajjoul, H.; Bisinoti, M. C. Humic-like acids from hydrochars: Study of the metal complexation properties compared with humic acids from anthropogenic soils using PARAFAC and time-resolved fluorescence. *Sci. Total Environ.* **2020**, *722*, No. 137815.

(26) Melendez-Perez, J. J.; Martínez-Mejia, M. J.; Eberlin, M. N. A reformulated aromaticity index equation under consideration for non-aromatic and non-condensed aromatic cyclic carbonyl compounds. *Org. Geochem.* **2016**, *95*, 29−33.

(27) Zherebker, A. Y.; Rukhovich, G. D.; Kharybin, O. N.; Fedoros, E. I.; Perminova, I. V.; Nikolaev, E. N. Fourier transform ion cyclotron resonance mass spectrometry for the analysis of molecular composition and batch-to-batch consistency of plant-derived polyphenolic ligands developed for biomedical application. *Rapid Commun. Mass Spectrom.* **2020**, *34*, No. e8850.

(28) Gao, Y.; Song, X.; Liu, K.; Li, T.; Zheng, W.; Wang, Y.; Liu, Z.; Zhang, M.; Chen, Q.; Li, Z.; Li, R.; Zheng, L.; Liu, W.; Miao, T. Mixture of controlled-release and conventional urea fertilizer application changed soil aggregate stability, humic acid molecular composition, and maize nitrogen uptake. *Sci. Total Environ.* **2021**, *789*, No. 147778.

(29) Wang, J.; Li, J.; Jiang, C.; Zhou, P.; Zhang, P.; Yu, J. The effect of manganese vacancy in birnessite-type MnO_2 on room-temperature oxidation of formaldehyde in air. *Appl. Catal., B* **2017**, *204*, 147−155.

(30) Lucht, K. P.; Mendoza-Cortes, J. L. Birnessite: A Layered Manganese Oxide To Capture Sunlight for Water-Splitting Catalysis. *J. Phys. Chem. C* **2015**, *119*, 22838−22846.

(31) Boyjoo, Y.; Rochard, G.; Giraudon, J.-M.; Liu, J.; Lamonier, J.-F. Mesoporous MnO_2 hollow spheres for enhanced catalytic oxidation of formaldehyde. *Sustainable Mater. Technol.* **2019**, *20*, No. e00091.

(32) Liang, M.; Guo, H.; Xiu, W. Effects of low molecular weight organic acids with different functional groups on arsenate adsorption on birnessite. *J. Hazard. Mater.* **2022**, *436*, No. 129108.

(33) Han, Z.; Wang, C.; Zou, X.; Chen, T.; Dong, S.; Zhao, Y.; Xie, J.; Liu, H. Diatomite-supported birnessite−type MnO_2 catalytic oxidation of formaldehyde: Preparation, performance and mechanism. *Appl. Surf. Sci.* **2020**, *502*, No. 144201.
(34) Wang, M.; Li, Y.; Zhang, Y.; Hu, X.; Li, Q.; Su, Y.; Zhao, W. Exploration of the H_2O_2 Oxidation Process and Characteristic Evaluation of Humic Acids from Two Typical Lignites. *ACS Omega* **2021**, *6*, 24051−24061.
(35) Zhang, S.; Yuan, L.; Li, W.; Lin, Z.; Li, Y.; Hu, S.; Zhao, B. Characterization of pH-fractionated humic acids derived from Chinese weathered coal. *Chemosphere* **2017**, *166*, 334−342.
(36) Ćwieląg-Piasecka, I.; Medyńska-Juraszek, A.; Jerzykiewicz, M.; Dębicka, M.; Bekier, J.; Jamroz, E.; Kawałko, D. Humic acid and biochar as specific sorbents of pesticides. *J. Soils Sediments* **2018**, *18*, 2692−2702.
(37) Ikeya, K.; Sleighter, R. L.; Hatcher, P. G.; Watanabe, A. Characterization of the chemical composition of soil humic acids using Fourier transform ion cyclotron resonance mass spectrometry. *Geochim. Cosmochim. Acta* **2015**, *153*, 169−182.
(38) Gomboš, M.; Tall, A.; Trpčevská, J.; Kandra, B.; Pavelkova, D.; Balejčíková, L. Sedimentation rate of soil microparticles. *Arabian J. Geosci.* **2018**, *11*, 635.
(39) Liu, J.; Hu, F.; Xu, C.; Wang, Z.; Ma, R.; Zhao, S.; Liu, G. Comparison of different methods for assessing effects of soil interparticle forces on aggregate stability. *Geoderma* **2021**, *385*, No. 114834.
(40) Malik, K. A.; Azam, F. Effect of humic acid on wheat (*Triticum aestivum* L.) seedling growth. *Environ. Exp. Bot.* **1985**, *25*, 245−252.
(41) Tuan, P. A.; Sun, M.; Nguyen, T.-N.; Park, S.; Ayele, B. T. Molecular mechanisms of seed germination. *Sprouted Grains* **2019**, 1−24.
(42) Bezuglova, O. S.; Polienko, E. A.; Gorovtsov, A. V.; Lyhman, V. A.; Pavlov, P. D. The effect of humic substances on winter wheat yield and fertility of ordinary chernozem. *Ann. Agrar. Sci.* **2017**, *15*, 239−242.

https://doi.org/10.1021/acsomega.2c06411
ACS Omega 2022, 7, 47192−47201